Contents lists available at ScienceDirect

# Brain, Behavior, & Immunity - Health

# Increased penetration of diphenhydramine in brain via proton-coupled organic cation antiporter in rats with lipopolysaccharide-induced inflammation

Atsushi Kawase [a,*], Taihei Chuma [a], Kota Irie [a], Akira Kazaoka [a], Asuka Kakuno [a], Naoya Matsuda [a], Hiroaki Shimada [a], Masahiro Iwaki [a,b,c]

[a] Department of Pharmacy, Faculty of Pharmacy, Kindai University, Osaka, Japan
[b] Pharmaceutical Research and Technology Institute, Kindai University, Osaka, Japan
[c] Antiaging Center, Kindai University, Osaka, Japan

## ARTICLE INFO

## ABSTRACT

Uptake transporters in brain microvascular endothelial cells (BMECs) are involved in the penetration of basic (cationic) drugs such as diphenhydramine (DPHM) into the brain. Lipopolysaccharide (LPS)-induced inflammation alters the expression levels and activities of uptake transporters, which change the penetration of DPHM into the brain. A brain microdialysis study showed that the unbound brain-to-plasma partition coefficient ($K_{p,uu,brain}$) for DPHM in LPS rats was approximately two times higher than that in control rats. The transcellular transport of DPHM to BMECs was increased when BMECs were cultured with serum from LPS rats. Compared with control rats or BMECs, the brain uptake of DPHM in LPS rats was increased and the intracellular accumulation of DPHM was increased under a high intracellular pH in BMECs from LPS rats, respectively. Treatment of BMECs with transporter inhibitors or inflammatory cytokines had little impact on the intracellular accumulation of DPHM in BMECs. This study suggests that LPS-induced inflammation promotes unidentified proton-coupled organic cation ($H^+$/OC) antiporters that improve the penetration of DPHM into rat brain via the blood-brain barrier.

## 1. Introduction

Efflux transporters such as P-glycoprotein (P-gp) and breast cancer resistance protein (BCRP) expressed in brain microvascular endothelial cells (BMECs) restrict the entry of substrates to the brain via the blood-brain barrier (BBB). BMECs also contain uptake transporters such as organic anion transporting polypeptides and organic cation transporters (OCT). Inflammation leads to alterations in the expression levels and activities of transporters, which changes the pharmacokinetics of some drugs (Fisher et al., 2009; Kawase et al., 2014; Liu et al., 2015; Uno et al., 2007). For example, lipopolysaccharide (LPS)-induced inflammation changes the expression levels of transporters in the liver because of the high susceptibility of the liver to inflammation (Cherrington et al., 2004; Kato et al., 2010). However, the effects of inflammation in the liver on the expression levels and activities of transporters in organs distant from the liver such as the brain remains unclear. Inflammation in the brain is related to Alzheimer's disease (Calsolaro and Edison, 2016; Heneka et al., 2015), Parkinson's disease (Perry, 2012), and Huntington's disease

(Pavese et al., 2006). Because transporter activities in the brain might determine the maintaining homeostasis and the occurrence of drug adverse reactions, it is important to clarify the effects of inflammation in the liver on the brain penetration of drugs via transporters. Previous reports suggest that the changes of P-gp activity in inflammation affect the brain penetration of P-gp substrates such as oseltamivir carboxylate (Morimoto et al., 2008; Ose et al., 2008; S et al., 2009). However, few studies have investigated the effects of hepatic inflammation on the penetration of basic (cationic) drugs into the brain via uptake transporters. Transporters such as OCT1/SLC22A1, OCT2/SLC22A2, OCT3/SLC22A3, multidrug and toxin extrusion (MATE/SLC47A), and novel organic cation transporter (OCTN1/SLC22A4 and OCTN2/SLC22A5) are involved the penetration of basic drugs into the brain (Kang et al., 2006; Kubo et al., 2013; Okura et al., 2007), and unidentified proton-coupled organic cation ($H^+$/OC) antiporters might be involved in the penetration of organic cations into the brain (Auvity et al., 2017; Chapy et al., 2015; Kitamura et al., 2014; Kurosawa et al., 2017; Suzuki et al., 2016).

The present study examined the effects of early phase in LPS-induced inflammation in rats on the penetration of diphenhydramine [2-(diphenylmethoxy)-*N,N*-dimethylethylamine (DPHM), a basic drug] into the brain via transporters in BMECs (Kuwayama et al., 2008; Sadiq et al., 2011). Higher concentrations of DPHM were observed in the brain compared with the plasma after the injection of DPHM to rats or guinea pigs (DILL and GLAZKO, 1949). After DPHM enters the brain, central $H_1$-receptors are activated, which results in drowsiness, sedation, dizziness, and convulsions (Gengo et al., 1989; Köppel et al., 1987; Nicholson, 1983). An increase in the penetration of DPHM into the brain increases the risk of neurological side effects induced by DPHM. To clarify the effects of inflammation on the brain penetration of basic drugs such as DPHM, we examined the effect of inflammation on the BBB transport of DPHM by *in vivo* brain microdialysis and isolated BMECs. The elucidation of effects of acute inflammation on the brain penetration of DPHM could help us better understand the relation between the changes of BBB function in inflammation and the brain penetration of basic drugs.

## 2. Materials and methods

### 2.1. Animals

Eight-week-old male Wistar rats were obtained from Japan SLC (Shizuoka, Japan). The rats were housed in an air-conditioned room at $22 \pm 0.5\ °C$ and relative air humidity of $55 \pm 10\%$ with a 12-h lighting schedule (7:00 a.m.−7:00 p.m.) and had free access to standard laboratory food (MF; Oriental Yeast Co., Ltd., Tokyo, Japan). The protocol was approved by the Committee for the Care and Use of Laboratory Animals of the Faculty of Pharmacy of Kindai University (Osaka, Japan).

### 2.2. Chemicals and reagents

LPS, DPHM, Evans blue, Sepasol-RNA I Super G, and Dulbecco's modified Eagle medium (DMEM) were from Nacalai Tesque (Kyoto, Japan). Decynium 22 (D22, 1,1′-diethyl-2,2′-cyanine iodide), pyrimethamine (PYR), recombinant human tumor necrosis factor-α (TNF-α), and recombinant human interleukin-1β (IL-1β) were from R&D Systems (Minneapolis, MN, USA). ReverTra Ace was from Toyobo Life Science (Osaka, Japan). Fast SYBR Green Master Mix and BCA protein assay kit were from Thermo Fisher Scientific (Waltham, MA, USA). DPHM-d₃, primers and endothelial cell growth supplement were from Sigma-Aldrich (St. Louis, MO, USA). Lucifer yellow CH dilithium salt and Transaminase CII Test kits Test were obtained from Fujifilm Wako Pure Chemical (Osaka, Japan). All other chemicals and solvents were of MS grade or the highest commercially available purity.

### 2.3. Measurement of BBB permeability

BBB permeability was evaluated by measuring the fluorescein intensity of Evans blue extravasation. Rats were treated with LPS (5 mg/kg, intraperitoneal [i.p.]) (Kato et al., 2008; S et al., 2017) or saline as a control. A 2% Evans blue in saline was injected i.p. (4 ml/kg) 6 h after LPS or saline treatments. Brains were excised from rats euthanized by sodium pentobarbital 1 h after Evans blue treatment. Brains were homogenized with 3 ml of 50% TCA and then centrifuged for 20 min at 10,000 × g. The supernatant was diluted in 4 vol of ethanol. Fluorescence intensity was measured (Ex 620 nm, Em 680 nm) using an SH-9000 lab fluorescent microplate reader (Corona Electric Co., Ibaraki, Japan).

### 2.4. Brain microdialysis

The concentration of unbound DPHM in the brain was determined by brain microdialysis as previously described with minor modifications (Sadiq et al., 2011). Rats anesthetized with pentobarbital were fixed with a brain stereotaxis apparatus (SR-5R-HT, Narishige, Tokyo, Japan) and the skull was exposed by making a midline incision. A hole was drilled

2.7 mm lateral, 0.8 mm anterior to the bregma, and 3.8 mm ventral to the surface of the brain. An AG-X guide cannula (Eicom, Kyoto, Japan) was implanted into the striatum and fixed to the skull by a screw and dental cement (Unifast III, GC, Tokyo, Japan). An A-I-8-03 (3 mm) probe was inserted after fixing the guide cannula. The probe was perfused with Ringer solution before insertion. The inlet and outlet were then sealed to prevent air from entering the probes. Rats were placed in a cage for freely moving animals with free access to water and food and were given 24 h to recover.

Rats implanted with a guide cannula were treated with LPS (5 mg/kg, i.p.) or saline as a control. The LPS dose of 5 mg/kg were chosen to exhibit relatively high levels of cytokine production 5 h after LPS treatment (Lee et al., 2012; Luster et al., 1994). There are also a lot of reports of the physiological condition after treatments of 5 mg/kg LPS (McKenna et al., 2018; Somann et al., 2019; Vos et al., 1997; Wedn et al., 2020a, 2020b). The plasma levels of aspartate transaminase (AST) and alanine transaminase (ALT) were determined by Transaminase CII Test kits. Rats received an injection of DPHM 6 h after LPS or saline treatments. DPHM was administered to rats as a 234 µg/min/kg constant rate intravenous infusion over 5 min and then as a 30 µg/min/kg constant rate intravenous infusion over 180 min with a syringe driver (ESP-32, Eicom). The probe was perfused with Ringer solution at a flow rate of 1 µl/min. The perfusates were collected sequentially every 10 min. Blood samples were collected from the tail vein at 0, 5, 15, 25, 45, 65, 85, 115, 145, 175, and 180 min after the initiation of DPHM infusion. Blood was collected in heparinized tubes and centrifuged for 10 min at $3000 \times g$. Perfusates and plasma samples were diluted 5-fold with Ringer solution and saline, respectively, and then stored at $-30\ °C$ until analysis.

### 2.5. Determination of plasma protein binding

After 400 µl plasma was collected at 180 min after DPHM infusion, an *in vitro* protein binding assay for DPHM was performed by the ultrafiltration method using the Centrifree Ultrafiltration Device (Merck, Kenilworth, NJ, USA). After the centrifugation of samples at $3000 \times g$ for 10 min, the concentrations of unbound DPHM in filtrates were measured by liquid chromatographic-tandem mass spectrometry (LC-MS/MS).

### 2.6. Data analysis of brain microdialysis

The recovery of DPHM was estimated by retrodialysis with DPHM for each probe (Bouw and Hammarlund-Udenaes, 1998). Retrodialysis was performed at a 1 µl/min flow rate of DPHM (30 ng/ml) for 50 min. Recovery was calculated as

$$Recovery = \frac{C_{in} - C_{out}}{C_{in}}$$

where $C_{in}$ is the concentration of DPHM in the perfusate and $C_{out}$ is the concentration of DPHM in the dialysate.

The concentration of unbound drug in the brain was calculated as

$$C_{u,brain} = \frac{C_{dialysate}}{Recovery}$$

The unbound brain-to-plasma partition coefficient ($K_{p,uu,brain}$) for DPHM was calculated as

$$K_{p,uu,brain} = \frac{C_{u,brain}}{C_{u,plasma}}$$

where $C_{u,brain}$ and $C_{u,plasma}$ are the mean unbound DPHM concentrations in the brain and plasma at 70–180 min after the initiation of DPHM infusion, respectively.

## 2.7. BMEC isolation and primary culture

BMECs were isolated from control and LPS rats as described previously (Assmann et al., 2017). Viability, as determined by trypan blue exclusion, was above 90%. BMECs were seeded at $1 \times 10^5$ cells/cm$^2$ on collagen-coated Transwell inserts (pore size; 0.4 μm) in 24-well plates (Corning, Corning, NY, USA) or collagen-coated 96-well plates (Sumitomo Bakelite, Tokyo, Japan) in DMEM supplemented with 10% fetal bovine serum (FBS), 100 U/ml penicillin, 100 μg/ml streptomycin, and 30 μg/ml endothelial cell growth supplement. Medium volumes of apical and basolateral compartments were 100 μl and 600 μl, respectively. Plates were incubated at 37 °C in the presence of 5% CO$_2$ and 95% air.

## 2.8. Determination of mRNA levels by real-time reverse transcriptase polymerase chain reaction (RT-PCR)

Total RNA was extracted from the livers or BMECs of control and LPS rats using Sepasol-RNA I Super G. mRNA expression levels were measured by RT-PCR as described previously (Kawase et al., 2008). The oligonucleotide sequences for mRNA target are shown in Table 1. Data were analyzed using StepOne Software (Thermo Fisher) using the multiplex comparative method.

## 2.9. Transport study in BMECs

Isolated BMECs were cultured for 2 days and medium was replaced with fresh medium containing 5% FBS and 5% serum from control or LPS rats. After stimulation with serum from control or LPS rats for 2 days, BMECs were used to study the transport of DPHM from the apical to basolateral compartments. Twenty-μl samples were taken from basolateral compartments at 1, 2, and 3 h after DPHM treatment (30 μM) in the apical compartments. Lucifer yellow CH dilithium, a permeable marker of tight junctions, was added to the apical compartment of the Transwell insert at 40 μg/ml in serum-free DMEM. After a 40-min incubation, medium in the basolateral compartment was collected and the fluorescence of Lucifer yellow was measured (Ex/Em: 428/536). The concentrations of DPHM were measured by LC-MS/MS. Permeability expressed as the apparent permeability ($P_{app}$) in cm/s was calculated as

$$P_{app} = \frac{dQ/dt}{A \times C_0}$$

**Table 1**
Primer sequences used in RT-PCR assays.

| Gene | Primer sequence (5′–3′) |
| --- | --- |
| Oct1 (SLC22A1) | Forward: CCAATAGCGGCCTCGAATCT |
| | Reverse: TGCAGCTCATGCGGGATAAA |
| Oct2 (SLC22A2) | Forward: TGAGGACGCTGGCAAGAAAT |
| | Reverse: AGAACAGAGCTCGTGAACCAAT |
| Oct3 (SLC22A3) | Forward: TATGCAGCGGACAGATACGG |
| | Reverse: AAAATTCGGTGCAAACGCCA |
| Mate1 (SLC47A1) | Forward: TGCTGTCTGGCTTTCAAGAG |
| | Reverse: TAACCGCAATTGCCAGTGTG |
| Octn1 (SLC22A4) | Forward: AAGCCGCAAAGATGAATGGC |
| | Reverse: TTGTGGCAATGTTCCGAGTC |
| Octn2 (SLC22A5) | Forward: ACTACGTGGCAGCATTTGTC |
| | Reverse: TATGCAAACAGAGGCAGCAC |
| Mdr1a | Forward: AAGGGGCTACAGGGTCTAGG |
| | Reverse: AGTGTCAATTGCCAGCCGTA |
| Mdr1b | Forward: GTGTCACGTGAGGTCGTGAT |
| | Reverse: TCCCGAATATGCCAACAGCA |
| IL-1β | Forward: TGACCCATGTGAGCTGAAAG |
| | Reverse: TCGTTGCTTGTCTCTCCTTG |
| IL-6 | Forward: TGCCACTTGTGTGCTAAAGG |
| | Reverse: CATGGTTTGTCTTCCACACG |
| TNF-α | Forward: GAAAGGGAATTGTGGCTCTG |
| | Reverse: TTCAGCGTCTCGTGTGTTTC |
| β-actin | Forward: GATCAAGATCATTGCTCCTCCTG |
| | Reverse: AGGGTGTAAAACGCAGCTCA |

where $dQ/dt$ is the transport rate of DPHM to the basolateral compartment, $A$ is the surface area of the monolayer, and $C_0$ is the initial concentration of DPHM in the apical compartment. The transport rate of DPHM was calculated by linear regression analysis using GraphPad Prism software version 5 (GraphPad Software, Inc., La Jolla, CA, USA).

## 2.10. Brain uptake index

To evaluate the brain uptake of DPHM in control and LPS rats, the brain uptake index (BUI), a single pass method, was performed as described previously (Oldendorf, 1970, 1981). First, 100 μl DPHM (3 μg/ml) was injected into the carotid artery of control and LPS rats in less than 0.5 s under anesthesia with pentobarbital. Rats were sacrificed by decapitation first-pass 13 s after DPHM treatment and brains were removed. Brains were homogenized in 5 vol of phosphate-buffered saline (PBS). An equal volume of acetonitrile was added to the homogenates for deproteinization. After centrifugation at $1200 \times g$ for 10 min, the DPHM concentrations in supernatants were determined. The percentage BUI was calculated using the following equation.

$$BUI = \frac{X_{DPHM, \, brain}}{X_{DPHM, \, injectate}} \times 100$$

where $X_{DPHM, \, brain}$ and $X_{DPHM, \, injectate}$ were the amounts of DPHM in the brain and injectate, respectively.

## 2.11. Uptake study in BMECs

BMECs cultivated for 24 h were washed twice with 100 μl PBS and preincubated with transport buffer (pH 7.4) containing 125 mM NaCl, 25 mM HEPES, 4.8 mM KCl, 1.2 mM D-glucose, 1.2 mM CaCl$_2$, and 1.2 mM KH$_2$PO$_4$ for 20 min. In the transporter inhibition study, BMECs were preincubated with D22 (1 μM), an OCT inhibitor (Hayer-Zillgen et al., 2002), or PYR (1 μM), a MATE inhibitor (Ito et al., 2010), for 20 min to evaluate the OCT- or MATE-mediated transport of DPHM. The effects of a proton gradient across the cell membrane on DPHM uptake were examined to evaluate the H$^+$/OC antiporter-mediated transport of DPHM. The intracellular pH (pHi) was reduced by preincubation with 30 mM NH$_4$Cl for 20 min and an exchange of transport buffer to generate a proton gradient (Shimomura et al., 2013){FormattingCitation}{FormattinCitation}. To clarify the effects of inflammatory cytokines on the H$^+$/OC antiporter-mediated transporter of DPHM, TNF-α or IL-1β at concentrations of 0.1, 0.3, 1, 3, 10, and 30 ng/ml were added 2 h after the seeding of BMECs from control rats. The DPHM uptake studies were performed 24 h after cytokine treatment. The cytokine doses were set by plasma concentrations after LPS treatment (Diao et al., 2010; Virdis et al., 2005).

The cells were incubated at 37 °C for 30 s after the addition of DPHM (30 μM) to initiate uptake. The medium was removed and then the cells were washed twice with 100 μl ice-cold PBS. The cell lysates were obtained by sonication for 2 min after the addition of 50 μl PBS with 2% Triton X-100.

## 2.12. Determination of DPHM concentrations by LC-MS/MS

The 10 μl diluted perfusate, plasma, brains, and cell lysates were added to 10 μl 6.25 M NaOH, 10 μl 10 ng/ml DPHM-d$_3$ as an internal standard, and 1 ml diethyl ether, and were centrifuged at $2000 \times g$ for 10 min after vigorous mixing for 15 min. The supernatant was evaporated to dryness using a centrifugal evaporator (Tokyo Rikakikai, Tokyo, Japan). The residues were dissolved in 40 μl LC mobile phase and filtered with a 0.45-μm Millex-LH filter unit (Merck KGaA).

Aliquots of 10 μl were injected into the LC-MS/MS consisting of an LC system (UltiMate 3000 series, Thermo Scientific) and a TSQ Endura Triple Quadrupole Mass Spectrometer with electrospray ionization (Thermo Scientific). For data recording and analysis, Finnigan Xcalibur software (Thermo Scientific) was used. Analysis was performed using a

reversed-phase column (Inertsil ODS-3, 4.6 × 75 mm, 5 μm; GL Sciences, Tokyo, Japan). The column temperature was set at 40 °C and the auto-sampler was maintained at 10 °C. The mobile phase (5 mM ammonium formate (pH 3.4)/acetonitrile (70:30, *v/v*)) was pumped at a flow rate of 1.0 ml/min. Retention times of DPHM and DPHM-d$_3$ were 1.85 min. The eluate was transferred into the electrospray probe, starting at 1.0 min after injection, by switching the MS inlet valve. The conditions of electrospray ionization were set at 3500 V spray voltage, 280 °C capillary temperature with the nitrogen sheath and 10 arbitrary units of auxiliary gases. The MS scan was operated in the positive ionization mode. The selected reaction monitoring mode (SRM) was used with argon as the collision gas at 1.5 mTorr. The detection molecular ion selected was for precursor 256.0 m/z and product 167.3 m/z of DPHM and precursor 259.2 m/z and product 167.3 m/z of DPHM-d$_3$ with 15 V collision energy. The mass resolutions were set at 0.7 full width at half height (unit resolution). The obtained area of DPHM was normalized by the area of DPHM-d$_3$.

### 2.13. Statistical analysis

Differences between the mean parameter values in control and LPS rats were estimated using Student's *t*-test or ANOVA, followed by the Bonferroni test using GraphPad Prism software (GraphPad Software, Inc.). The threshold for significance was $p < 0.05$.

## 3. Results

### 3.1. The integrity of BBB tight junctions was maintained after LPS treatments

The plasma concentrations of AST and ALT as indicators of liver inflammation were measured (Table 2). In LPS rats, the approximately 2–3 times higher concentrations of AST and ALT were observed compared with those in control rats, indicating minor liver damage. To confirm the integrity of BBB tight junctions after LPS treatment, Evans blue extravasation into the brains of control and LPS rats was determined. Evans blue dye on the surface of brains from control and LPS rats was low (Fig. 1a). There was little change in the fluorescence intensity between control and LPS brains (Fig. 1b).

### 3.2. Brain penetration of DPHM was increased after LPS treatments

The concentrations of unbound DPHM in brains and plasma were determined by brain microdialysis. Time courses of $C_{u,brain}$ and $C_{u,plasma}$ of DPHM in control and LPS rats are shown in Fig. 2. At 60 min after the initiation of DPHM infusion, the $C_{u,brain}$ and $C_{u,plasma}$ of DPHM in control and LPS rats reached a steady state. The $C_{u,brain}$, $C_{u,plasma}$, and $K_{p,uu,brain}$ in the steady state were estimated from the results of Fig. 2 and the bound fraction of DPHM in the plasma is shown in Table 3. The $C_{u,plasma}$ of DPHM in LPS rats tended to be decreased compared with that in control rats. The $C_{u,brain}$ and protein binding of DPHM were unchanged between control and LPS rats. The $K_{p,uu,brain}$ in LPS rats was significantly increased compared with that in control rats.

### 3.3. TNF-α mRNA levels were increased, and transporters mRNA levels were unchanged in BMECs from LPS rats

To clarify the effects of LPS-induced inflammation on cytokine

**Table 2**
Plasma concentrations of AST and ALT in control and LPS rats.

| | Control | LPS |
|---|---|---|
| AST (U/L) | 66.5 ± 9.11 | 186 ± 14.0*** |
| ALT (U/L) | 23.0 ± 7.43 | 70.7 ± 15.1** |

The results are expressed as the mean ± SD (n = 4). *; $P < 0.05$ vs control.
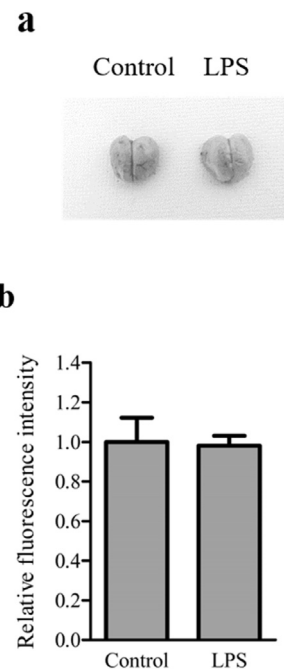


**Fig. 1.** Evans blue dye permeability assay for the integrity of BBB tight junctions after LPS treatment. The fluorescence intensity of Evans blue in brain homogenates was measured 1 h after the intraperitoneal injection of Evans blue to control and LPS rats. The results are expressed as the mean ± SD (n = 3–6).

production and transporter expression, the mRNA levels of cytokines and transporters in the liver and BMECs isolated from control and LPS rats were measured. In the liver, the mRNA levels of IL-1β and TNF-α were significantly increased by LPS-induced inflammation (Table 4). In the brain, significantly increased mRNA levels of TNF-α but not IL-1β and IL-6 were observed in LPS rats compared with control rats (Table 4). The mRNA levels of *Oct1* and *Octn2* in livers of LPS rats were significantly lower than in those from control rats (Table 5). The mRNA levels of *Mate1* and *Octn1* in livers of LPS rats tended to be decreased compared with those of control rats (Table 5). There were minimal differences in *Oct1*, *Oct2*, *Oct3*, *Mate1*, *Octn1*, *Octn2*, *Mdr1a,* and *Mdr1b* mRNA levels in the brains of control and LPS rats (Table 5).

### 3.4. Transcellular transport of DPHM to BMECs cultured with serum of LPS rats was elevated

We examined whether the addition of serum from LPS rats to BMECs affected the transport rate of DPHM to BMECs. Significantly higher concentrations of DPHM in the basolateral compartment of BMECs treated with serum from LPS rats were observed 3 h after DPHM treatments compared with those from control rats (Fig. 3a). Apparent permeability coefficient P$_{app}$ values of DPHM in BMECs treated with serum from control or LPS rats were $3.09 \times 10^{-6} \pm 4.84 \times 10^{-7}$ cm/s and $4.63 \times 10^{-6} \pm 0.94 \times 10^{-6}$ cm/s, respectively. P$_{app}$ values of DPHM in LPS rats were significantly higher compared with those in control rats ($p < 0.05$). The intracellular accumulation of DPHM in BMECs treated with serum from control or LPS rats was examined. A significantly higher accumulation of DPHM was observed in BMECs treated with serum from LPS rats compared with control rats (Fig. 3b).

### 3.5. Brain uptake of DPHM in LPS rats was increased and the intracellular accumulation of DPHM was increased under a high intracellular pH in BMECs from LPS rats

The transcellular transport of DPHM is involved in the process of uptake from the apical side into BMECs and efflux from BMECs to the
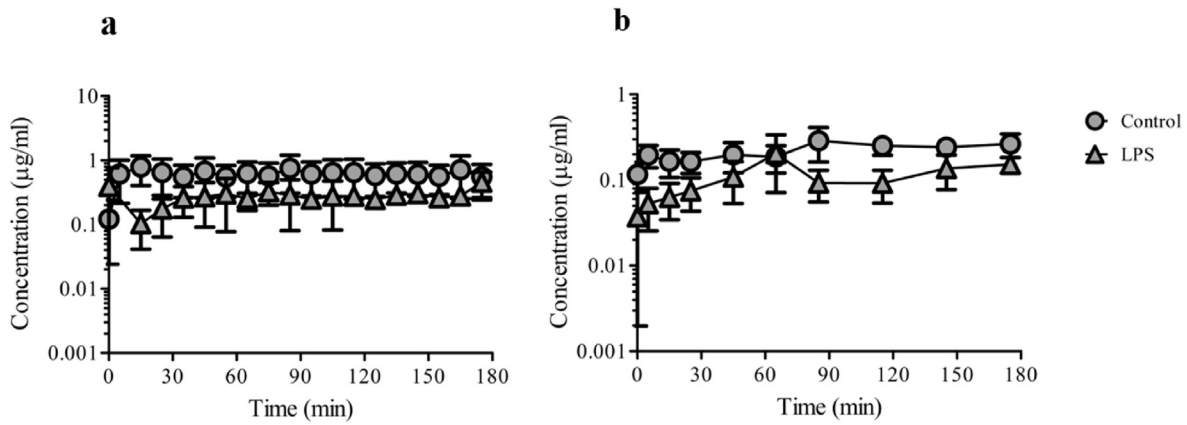
**Fig. 2.** Unbound DPHM concentrations in brain (a) and plasma (b) after the administration of DPHM to control and LPS rats. Rats received an DPHM injection 6 h after LPS or saline treatments. DPHM was administered to rats as a 234 μg/min/kg constant rate intravenous infusion over 5 min and then as a 30 μg/min/kg constant rate intravenous infusion over 180 min. The results are expressed as the mean ± SD (n = 3–4).

**Table 3**
$C_{u,brain}$, $C_{u,plasma}$, protein binding, and $K_{p,uu,brain}$ of DPHM after DPHM infusion to control and LPS rats.

| Parameter | Control | LPS |
|---|---|---|
| $C_{u,brain}$ (μg/ml) | 0.281 ± 0.048 | 0.253 ± 0.078 |
| $C_{u,plasma}$ (μg/ml) | 0.096 ± 0.030 | 0.033 ± 0.007 |
| Bound fraction in plasma (%) | 60.0 ± 6.76 | 77.2 ± 3.80 |
| $K_{p,uu,brain}$ | 3.24 ± 0.84 | 7.00 ± 0.77* |

The results are expressed as the mean ± SD (n = 3–4). *; $P < 0.05$ vs control.

**Table 4**
Relative mRNA levels of IL-1β, IL-6, and TNF-α in livers and brains between LPS and control rats.

| | | Control | LPS |
|---|---|---|---|
| Liver | IL-1β | 1.00 ± 0.33 | 5.67 ± 1.49* |
| | IL-6 | 1.00 ± 0.35 | 1.40 ± 0.31 |
| | TNF-α | 1.00 ± 0.26 | 22.1 ± 6.29* |
| Brain | IL-1β | 1.00 ± 0.23 | 0.48 ± 0.13 |
| | IL-6 | 1.00 ± 0.34 | 0.48 ± 0.17 |
| | TNF-α | 1.00 ± 0.16 | 24.0 ± 8.39* |

The results are expressed as the mean ± SD (n = 4–6). *; $P < 0.05$ vs control.

**Table 5**
Relative mRNA levels of *Oct1, Oct2, Oct3, Mate1, Octn1, Octn2, Mdr1a,* and *Mdr1b* in livers and BMECs between LPS and control rats.

| | | Control | LPS |
|---|---|---|---|
| Liver | *Oct1* | 1.00 ± 0.26 | 0.10 ± 0.05* |
| | *Mate1* | 1.00 ± 0.50 | 0.42 ± 0.18 |
| | *Octn1* | 1.00 ± 0.20 | 0.44 ± 0.19 |
| | *Octn2* | 1.00 ± 0.34 | 0.12 ± 0.04* |
| BMECs | *Oct1* | 1.00 ± 0.19 | 1.21 ± 0.34 |
| | *Oct2* | 1.00 ± 0.36 | 1.63 ± 0.35 |
| | *Oct3* | 1.00 ± 0.24 | 1.06 ± 0.11 |
| | *Mate1* | 1.00 ± 0.27 | 1.68 ± 0.38 |
| | *Octn1* | 1.00 ± 0.19 | 1.00 ± 0.14 |
| | *Octn2* | 1.00 ± 0.18 | 0.87 ± 0.12 |
| | *Mdr1a* | 1.00 ± 0.11 | 1.07 ± 0.08 |
| | *Mdr1b* | 1.00 ± 0.05 | 1.09 ± 0.09 |

The results are expressed as the mean ± SD (n = 4–6). *; $P < 0.05$ vs control.

basolateral side. To clarify the effects of LPS-induced inflammation on the uptake process of DPHM into BMECs, the BUI method was performed in control and LPS rats. The uptake of diclofenac as a reference compound was similar between control and LPS rats (data not shown). The BUI of control and LPS rats was 21.4 ± 3.6% and 49.2 ± 13.9%, respectively. To
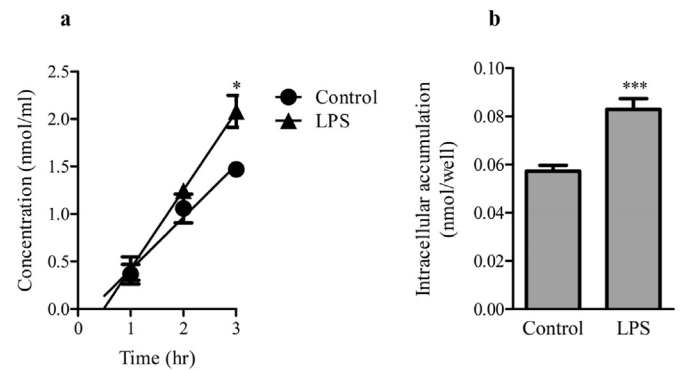


**Fig. 3.** DPHM transport across BMECs (a) and intracellular accumulation of DPHM into BMECs (b) cultured with medium containing serum from control or LPS rats. The concentrations of DPHM in the medium collected from the basolateral side at 1, 2, and 3 h (a) and in BMECs at 30 s (b) after DPHM treatment (30 μM) were determined. The results are expressed as the mean ± SEM (n = 4). *; $p < 0.05$ and ***; $p < 0.001$.

clarify further the effects of LPS treatment on DPHM transport into BMECs, the effects of transporter inhibitors, proton gradient, and inflammatory cytokines were investigated. The intracellular accumulation of DPHM via transporters in BMECs with D22 (an OCT inhibitor) or PYR (a MATE inhibitor) is shown in Fig. 4. Co-treatment with D22 or PYR had little effect on the intracellular accumulation of DPHM in BMECs from control or LPS rats (Fig. 4). To clarify whether the activity of the $H^+$/OC antiporter was altered in LPS rats, the effect of reducing the pHi on the intracellular accumulation of DPHM in BMECs was determined. The intracellular accumulation of DPHM was increased by the reduction of the pHi in BMECs from control and LPS rats (Fig. 5). In particular, the DPHM uptake was higher in the presence of a low pHi in BMECs from LPS rats compared with those of control rats. Next, we examined the intracellular accumulation of DPHM in BMECs after the treatment of BMECs with IL-1β or TNF-α, because the mRNA levels of IL-1β and TNF-α in the livers and brains of LPS rats were significantly increased (Table 4). IL-1β and TNF-α had little effect on DPHM uptake into BMECs (Fig. 6). Short-term cytokine treatment (3 h) had no effect on the intracellular accumulation of DPHM in BMECs (data not shown).

## 4. Discussion

After the injection of DPHM to rats or guinea pigs, higher total concentrations of DPHM were observed in the brain compared with the plasma (Dill and Glazko, 1949). A previous report demonstrated that the
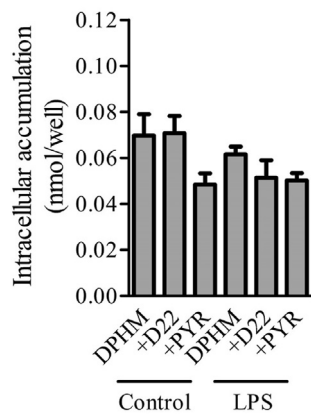
**Fig. 4.** Intracellular accumulation of DPHM for 30 s in BMECs from control and LPS rats treated with D22 or PYR. The concentrations of DPHM in BMECs were determined. The results are expressed as the mean ± SEM (n = 12–24).
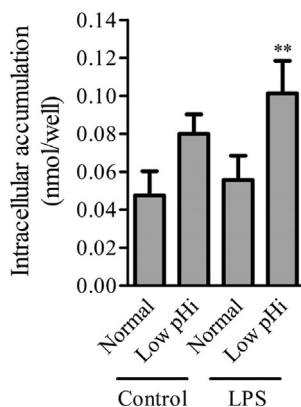


**Fig. 5.** Intracellular accumulation of DPHM for 30 s in BMECs of control and LPS rats with a reduction in the pHi. The concentrations of DPHM in BMECs were determined. The results are expressed as the mean ± SEM (n = 16). **; $p < 0.01$ vs the normal pHi LPS group.
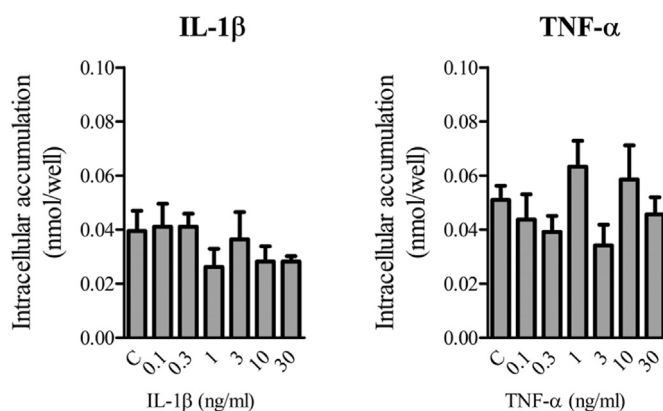


**Fig. 6.** Intracellular accumulation of DPHM for 30 s in BMECs of control and LPS rats treated with IL-1β or TNF-α. The concentrations of DPHM in BMECs were determined. The results are expressed as the mean ± SEM (n = 8–16).

unbound concentration of DPHM in sheep was two times higher in the brain than in the blood (Au-Yeung et al., 2006), suggesting that transporter-mediated transport was involved in the brain penetration of DPHM. The $K_{p,uu,brain}$ of DPHM in control rats was higher than 1 as previously reported (Sadiq et al., 2011; Shaffer et al., 2014) similar to the

results shown in Table 3.

In LPS rats, the $K_{p,uu,brain}$ of DPHM was significantly increased (approximately two times higher than the control value), although there was little change in the protein binding of DPHM between control and LPS rats (Table 3). These results suggested that LPS-induced inflammation might alter the protein expression and/or activities of transporters involved in DPHM transport and improve the brain penetration of DPHM across the BBB. To clarify whether the serum components of LPS rats affected the transport activity for DPHM in control BMECs, the uptake and intracellular accumulation of DPHM in BMECs were examined after the exposure of serum from control or LPS rats to control BMECs for 2 days (Fig. 3). The results of Fig. 3 suggest that the serum components of LPS rats increase the uptake and intracellular accumulation of DPHM in BMECs. Also, the results of BUI study show that the increases of DPHM uptake in LPS rats occurred.

Several reports demonstrated that LPS treatment affected the hepatic expression and activity of transporters (Cherrington et al., 2004; Donner et al., 2004; Hartmann et al., 2005). In accord with previous reports, the mRNA levels of transporters such as Oct1 and Octn2 in the livers of LPS rats were significantly decreased (Cherrington et al., 2004). However, the effects of LPS-induced inflammation on brain transporters, particularly uptake transporters, are unclear. Transporter mRNA levels were similar in the brains of control and LPS rats (Table 5), suggesting that the effect of LPS-induced inflammation on the mRNA levels of transporters was higher in the liver compared with the brain. We previously demonstrated that transporter expressions were different in organs including the liver, kidney, small intestine, and brain in adjuvant-induced arthritis rats, an inflammatory animal model (Kawase et al., 2014). For example, the expression levels of efflux transporters such as P-gp in kidneys were increased and those in livers were decreased in adjuvant-induced arthritic rats. The changes of transporter levels in brains of LPS rats could differ from those in livers. There are little reports on the changes of uptake transporter levels in brains, although the changes of uptake transporter levels in livers of LPS-induced inflammation have been reported (Bolder et al., 2006; Cherrington et al., 2004; Hartmann et al., 2002). The results in Table 5 suggest that LPS-induced inflammation has the higher impacts on the transporter mRNA levels in livers compared with those in brains 6 h after LPS treatments. Protein levels of uptake transporters in BMECs were undetectable by targeted proteomics as previous shown (Kawase et al, 2018, 2019). The transcriptional activities of Oct1 and Octn2 are regulated by peroxisome proliferator agonist receptor-alpha (PPARα) (Luo et al., 2014; Nie et al., 2005; Wen et al., 2010). A previous report showed that hepatic PPARα expression was reduced by LPS treatment (Sung et al., 2004), suggesting hepatic Oct1 and Octn2 mRNA might be decreased by a reduction in hepatic PPARα in LPS rats.

To clarify the effects of LPS-induced inflammation on the transporter-mediated transport of DPHM, changes in the intracellular accumulation of DPHM in BMECs were investigated using inhibitors for transporters, proton gradient, and inflammatory cytokines. The intracellular uptake of amantadine, a substrate of OCT1 and OCT2 (Goralski et al., 2002; Wright et al., 2004), was inhibited by DPHM, suggesting that OCT1 and/or OCT2 were partly involved in the brain penetration of DPHM (Spector, 1988). The expressions of OCT1 and OCT2 were localized to the luminal side of BMECs similar to P-gp (Lin et al., 2010). The expression of OCT3 is restricted to glial cells and neuronal cells but not BMECs (Gasser et al., 2017). The detailed localization of MATE is undetermined, although it was reported to be expressed in the BBB (Geier et al., 2013). DPHM uptake into BMECs was similar between control and LPS rats co-treated with D22 or PYR (Fig. 4). Changes in OCT and MATE in LPS rats might not be related to the increased brain penetration of DPHM, because DPHM uptake into BMECs of control and LPS rats was unchanged by D22 and PYR. Previous reports demonstrated that undefined H$^+$/OC antiporters might participate in the transporter-mediated transport of DPHM to the brain using a human brain capillary endothelial cell line (Chapy et al., 2015; Kurosawa et al., 2017; Shimomura et al., 2013). To clarify

the effects of LPS treatment on the activity of H$^+$/OC antiporters, DPHM uptake was examined using BMECs with a generated proton gradient. The elevation of the pHi of BMECs increased DPHM uptake into BMECs from control and LPS rats (Fig. 5), suggesting that the elevation of pHi in BMECs facilitates H$^+$/OC antiporters in BMECs. Of note, a significantly higher uptake of DPHM into BMECs from LPS rats was observed compared with control rats. These results suggested that the increased activity of H$^+$/OC antiporters in the BMECs of LPS rats might increase the brain penetration of DPHM. Alterations in the mRNA and protein expression levels of H$^+$/OC antiporters could not be determined, because the unidentified H$^+$/OC antiporters are not well-characterized transporters. The enhanced expression and/or activity of H$^+$/OC antiporters in LPS-induced inflammation might increase the $K_{p,uu,brain}$ of DPHM in LPS rats. Inflammatory cytokines such as IL-1β, IL-6, and TNF-α affected the expression levels of transporters in the brain (Bauer et al., 2007; Miller et al., 2008; Poller et al., 2010). Secreted cytokine levels often correlate with the mRNA levels of cytokines (Shebl et al., 2010) and the plasma levels of IL-6 and TNF-α were increased by LPS (Foster et al., 1993; Nežić et al., 2009; Yao et al., 1997). Qin et al. demonstrated that increased TNF-α levels in the brain after LPS treatment (5 mg/kg) were sustained for 10 months whereas they quickly returned to control levels after 1 day in the liver (Qin et al., 2007). Yu et al. demonstrated that TNF-α increased the expression and activity of P-gp in BMECs (Yu et al., 2007). Somann et al. demonstrated that the plasma levels of IL-10 increased 40 min after LPS treatments (5 mg/kg), following TNF-α, granulocyte macrophage colony-stimulating factor, IL-17, IL-6, IL-22, and interferon-γ increased above baseline up to at least 300 min. Therefore, we determined whether inflammatory cytokines increased by LPS treatment had an effect on DPHM uptake into BMECs. The treatments of BMECs with IL-1β or TNF-α had no impact on DPHM uptake into BMECs (Fig. 6). The activity of H$^+$/OC antiporters in BMECs was not directly affected by the TNF-α treatment of BMECs, although TNF-α mRNA was markedly elevated in the brains of rats treated with LPS.

Previous reports of other groups demonstrated that the various drugs could be substrates for H$^+$/OC antiporters. For example, oxycodone, pyrilamine, tramadol, pramipexole, clonidine, and varenicline as well as DPHM ware transported by H$^+$/OC antiporters (Higuchi et al., 2015; Kitamura et al., 2016; Kurosawa et al, 2017, 2018; Nakazawa et al., 2010; Okura et al., 2008; Wang et al., 2017). Acute inflammation could have impacts on the brain penetration of these substrates as well as DPHM.

In conclusion, LPS-induced inflammation increases the activity of H$^+$/OC antiporters in BMECs, which might increase the penetration of substrates such as DPHM into the brain.

## Declaration of competing interest

None.

## References

Assmann, J., Müller, K., Wenzel, J., Walther, T., Brands, J., Thornton, P., Allan, S., Schwaninger, M., 2017. Isolation and cultivation of primary brain endothelial cells from adult mice. BIO-PROTOCOL 7. https://doi.org/10.21769/BioProtoc.2294.

Au-Yeung, S.C.S., Rurak, D.W., Gruber, N., Riggs, K.W., 2006. A pharmacokinetic study of diphenhydramine transport across the blood-brain barrier in adult sheep: potential involvement of a carrier-mediated mechanism. Drug Metab. Dispos. 34, 955–960. https://doi.org/10.1124/dmd.105.007898.

Auvity, S., Chapy, H., Goutal, S., Caillé, F., Hosten, B., Smirnova, M., Declèves, X., Tournier, N., Cisternino, S., 2017. Diphenhydramine as a selective probe to study H$^+$-antiporter function at the blood–brain barrier: application to [$^{11}$C]

diphenhydramine positron emission tomography imaging. J. Cerebr. Blood Flow Metab. 37, 2185–2195. https://doi.org/10.1177/0271678X16662042.

Bauer, B., Hartz, A.M.S., Miller, D.S., 2007. Tumor necrosis factor α and endothelin-1 increase p-glycoprotein expression and transport activity at the blood-brain barrier. Mol. Pharmacol. https://doi.org/10.1124/mol.106.029512.

Bolder, U., Jeschke, M.G., Landmann, L., Wolf, F., De Sousa, C., Schlitt, H.J., Przkora, R., 2006. Heat stress enhances recovery of hepatocyte bile acid and organic anion transporters in endotoxemic rats by multiple mechanisms. Cell Stress Chaperones 11, 89–100. https://doi.org/10.1379/CSC-143R.1.

Bouw, M.R., Hammarlund-Udenaes, M., 1998. Methodological aspects of the use of a calibrator in in vivo microdialysis-further development of the retrodialysis method. Pharm. Res. (N. Y.) 15, 1673–1679.

Calsolaro, V., Edison, P., 2016. Neuroinflammation in Alzheimer's disease: current evidence and future directions. Alzheimer's Dementia 12, 719–732. https://doi.org/10.1016/j.jalz.2016.02.010.

Chapy, H., Goracci, L., Vayer, P., Parmentier, Y., Carrupt, P.A., Declèves, X., Scherrmann, J.M., Cisternino, S., Cruciani, G., 2015. Pharmacophore-based discovery of inhibitors of a novel drug/proton antiporter in human brain endothelial hCMEC/D3 cell line. Br. J. Pharmacol. https://doi.org/10.1111/bph.13258.

Cherrington, N.J., Slitt, A.L., Li, N., Klaassen, C.D., 2004. Lipopolysaccharide-mediated regulation of hepatic transporter mRNA levels in rats. Drug Metab. Dispos. 32, 734–741.

Diao, L., Li, N., Brayman, T.G., Hotz, K.J., Lai, Y., 2010. Regulation of MRP2/ABCC2 and BSEP/ABCB11 expression in sandwich cultured human and rat hepatocytes exposed to inflammatory cytokines TNF-α, IL-6, and IL-1β. J. Biol. Chem. https://doi.org/10.1074/jbc.M110.107805.

DILL, W.A., GLAZKO, A.J., 1949. Biochemical studies on diphenhydramine (benadryl) chemical determination of diphenhydramine. J. Biol. Chem. 179, 395–401.

Donner, M.G., Warskulat, U., Saha, N., Häussinger, D., 2004. Enhanced expression of basolateral multidrug resistance protein isoforms Mrp3 and Mrp5 in rat liver by LPS. Biol. Chem. 385 https://doi.org/10.1515/BC.2004.029.

Fisher, C.D., Lickteig, A.J., Augustine, L.M., Oude Elferink, R.P.J., Besselsen, D.G., Erickson, R.P., Cherrington, N.J., 2009. Experimental non-alcoholic fatty liver disease results in decreased hepatic uptake transporter expression and function in rats. Eur. J. Pharmacol. 613, 119–127. https://doi.org/10.1016/j.ejphar.2009.04.002.

Foster, S.J., McCormick, L.M., Ntolosi, B.A., Campbell, J., 1993. Production of TNF alpha by LPS-stimulated murine, rat and human blood and its pharmacological modulation. Agents Actions 38, C77–C79. Spec No.

Gasser, P.J., Hurley, M.M., Chan, J., Pickel, V.M., 2017. Organic cation transporter 3 (OCT3) is localized to intracellular and surface membranes in select glial and neuronal cells within the basolateral amygdaloid complex of both rats and mice. Brain Struct. Funct. 222, 1913–1928. https://doi.org/10.1007/s00429-016-1315-9.

Geier, E.G., Chen, E.C., Webb, A., Papp, A.C., Yee, S.W., Sadee, W., Giacomini, K.M., 2013. Profiling solute carrier transporters in the human blood-brain barrier. Clin. Pharmacol. Ther. https://doi.org/10.1038/clpt.2013.175.

Gengo, F., Gabos, C., Miller, J.K., 1989. The pharmacodynamics of diphenhydramine-induced drowsiness and changes in mental performance. Clin. Pharmacol. Ther. 45, 15–21.

Goralski, K.B., Lou, G., Prowse, M.T., Gorboulev, V., Volk, C., Koepsell, H., Sitar, D.S., 2002. The cation transporters rOCT1 and rOCT2 interact with bicarbonate but play only a minor role for amantadine uptake into rat renal proximal tubules. J. Pharmacol. Exp. Therapeut. 303, 959–968. https://doi.org/10.1124/jpet.102.038885.

Hartmann, G., Cheung, A.K.Y., Piquette-Miller, M., 2002. Inflammatory cytokines, but not bile acids, regulate expression of murine hepatic anion transporters in endotoxemia. J. Pharmacol. Exp. Therapeut. 303, 273–281. https://doi.org/10.1124/jpet.102.039404.

Hartmann, G., Vassileva, V., Piquette-Miller, M., 2005. Impact of endotoxin-induced changes in P-glycoprotein expression on disposition of doxorubicin in mice. Drug Metab. Dispos. 33, 820–828. https://doi.org/10.1124/dmd.104.002568.

Hayer-Zillgen, M., Brüss, M., Bönisch, H., 2002. Expression and pharmacological profile of the human organic cation transporters hOCT1, hOCT2 and hOCT3. Br. J. Pharmacol. https://doi.org/10.1038/sj.bjp.0704785.

Heneka, M.T., Carson, M.J., El Khoury, J., Landreth, G.E., Brosseron, F., Feinstein, D.L., Jacobs, A.H., Wyss-Coray, T., Vitorica, J., Ransohoff, R.M., Herrup, K., Frautschy, S.A., Finsen, B., Brown, G.C., Verkhratsky, A., Yamanaka, K., Koistinaho, J., Latz, E., Halle, A., Petzold, G.C., Town, T., Morgan, D., Shinohara, M.L., Perry, V.H., Holmes, C., Bazan, N.G., Brooks, D.J., Hunot, S., Joseph, B., Deigendesch, N., Garaschuk, O., Boddeke, E., Dinarello, C.A., Breitner, J.C., Cole, G.M., Golenbock, D.T., Kummer, M.P., 2015. Neuroinflammation in Alzheimer's disease. Lancet Neurol. 14, 388–405. https://doi.org/10.1016/S1474-4422(15)70016-5.

Higuchi, K., Kitamura, A., Okura, T., Deguchi, Y., 2015. Memantine transport by a proton-coupled organic cation antiporter in hCMEC/D3 cells, an in vitro human blood-brain barrier model. Drug Metabol. Pharmacokinet. 30, 182–187. https://doi.org/10.1016/j.dmpk.2014.12.006.

Ito, S., Kusuhara, H., Kuroiwa, Y., Wu, C., Moriyama, Y., Inoue, K., Kondo, T., Yuasa, H., Nakayama, H., Horita, S., Sugiyama, Y., 2010. Potent and specific inhibition of mMate1-mediated efflux of type I organic cations in the liver and kidney by pyrimethamine. J. Pharmacol. Exp. Therapeut. https://doi.org/10.1124/jpet.109.163642.

Kang, H.-J., Lee, S.-S., Lee, C.-H., Shim, J.-C., Shin, H.J., Liu, K.-H., Yoo, M.-A., Shin, J.-G., 2006. Neurotoxic pyridinium metabolites OF haloperidol are substrates OF human organic cation transporters. Drug Metab. Dispos. 34, 1145–1151. https://doi.org/10.1124/dmd.105.009126.

Kato, R., Moriguchi, J., Irie, T., Nakagawa, M., Kusukawa, Y., Matsumura, H., Ijiri, Y., Tanaka, K., 2010. Effects of lipopolysaccharide on P-glycoprotein expression and activity in the liver and kidneys. Eur. J. Pharmacol. 636, 155–158. https://doi.org/10.1016/j.ejphar.2010.03.024.

Kato, R., Yamashita, S., Moriguchi, J., Nakagawa, M., Tsukura, Y., Uchida, K., Amano, F., Hirotani, Y., Ijiri, Y., Tanaka, K., 2008. Changes of midazolam pharmacokinetics in Wistar rats treated with lipopolysaccharide: relationship between total CYP and CYP3A2. Innate Immun. https://doi.org/10.1177/1753425908095956.

Kawase, A., Fujii, A., Negoro, M., Akai, R., Ishikubo, M., Komura, H., Iwaki, M., 2008. Differences in cytochrome P450 and nuclear receptor mRNA levels in liver and small intestines between SD and DA rats. Drug Metabol. Pharmacokinet. 23, 196–206.

Kawase, A., Kazaoka, A., Yamamoto, R., Minakata, R., Shimada, H., Iwaki, M., 2019. Changes in transporters and metabolizing enzymes in the livers of rats with bile duct ligation. J. Pharm. Pharmaceut. Sci. 22, 457–465. https://doi.org/10.18433/jpps30637.

Kawase, A., Norikane, S., Okada, A., Adachi, M., Kato, Y., Iwaki, M., 2014. Distinct alterations in ATP-binding cassette transporter expression in liver, kidney, small intestine, and brain in adjuvant-induced arthritic rats. J. Pharmacol. Sci. 103, 2556–2564. https://doi.org/10.1002/jps.24043.

Kawase, A., Tateishi, S., Kazaoka, A., 2018. Profiling of hepatic metabolizing enzymes and nuclear receptors in rats with adjuvant arthritis by targeted proteomics. Biopharm Drug Dispos. 39, 308–314. https://doi.org/10.1002/bdd.2147.

Kitamura, A., Higuchi, K., Okura, T., Deguchi, Y., 2014. Transport characteristics of tramadol in the blood–brain barrier. J. Pharmacol. Sci. 103, 3335–3341. https://doi.org/10.1002/jps.24129.

Kitamura, A., Okura, T., Higuchi, K., Deguchi, Y., 2016. Cocktail-dosing microdialysis study to simultaneously assess delivery of multiple organic-cationic drugs to the brain. J. Pharmacol. Sci. 105, 935–940. https://doi.org/10.1002/jps.24691.

Köppel, C., Ibe, K., Tenczer, J., 1987. Clinical symptomatology of diphenhydramine overdose: an evaluation of 136 cases in 1982 to 1985. J. Toxicol. Clin. Toxicol. 25, 53–70.

Kubo, Y., Shimizu, Y., Kusagawa, Y., Akanuma, S.-I., Hosoya, K.-I., 2013. Propranolol transport across the inner blood–retinal barrier: potential involvement of a novel organic cation transporter. J. Pharmacol. Sci. 102, 3332–3342. https://doi.org/10.1002/jps.23535.

Kurosawa, T., Higuchi, K., Okura, T., Kobayashi, K., Kusuhara, H., Deguchi, Y., 2017. Involvement of proton-coupled organic cation antiporter in varenicline transport at blood-brain barrier of rats and in human brain capillary endothelial cells. J. Pharmacol. Sci. 106, 2576–2582. https://doi.org/10.1016/j.xphs.2017.04.032.

Kurosawa, T., Tega, Y., Higuchi, K., Yamaguchi, T., Nakakura, T., Mochizuki, T., Kusuhara, H., Kawabata, K., Deguchi, Y., 2018. Expression and functional characterization of drug transporters in brain microvascular endothelial cells derived from human induced pluripotent stem cells. Mol. Pharm. 15, 5546–5555. https://doi.org/10.1021/acs.molpharmaceut.8b00697.

Kuwayama, K., Inoue, H., Kanamori, T., Tsujikawa, K., Miyaguchi, H., Iwata, Y., Miyauchi, S., Kamo, N., Kishi, T., 2008. Uptake of 3,4-methylenedioxymethamphetamine and its related compounds by a proton-coupled transport system in Caco-2 cells. Biochim. Biophys. Acta Biomembr. 1778, 42–50. https://doi.org/10.1016/j.bbamem.2007.08.023.

Lee, S.H., Lee, E., Ko, Y.T., 2012. Anti-inflammatory effects of a methanol extract from Pulsatilla koreana in lipopolysaccharide-exposed rats. BMB Rep 45, 371–376. https://doi.org/10.5483/BMBRep.2012.45.6.018.

Lin, C.-J., Tai, Y., Huang, M.-T., Tsai, Y.-F., Hsu, H.-J., Tzen, K.-Y., Liou, H.-H., 2010. Cellular localization of the organic cation transporters, OCT1 and OCT2, in brain microvessel endothelial cells and its implication for MPTP transport across the blood-brain barrier and MPTP-induced dopaminergic toxicity in rodents. J. Neurochem. 114, 717–727. https://doi.org/10.1111/j.1471-4159.2010.06801.x.

Liu, J., Zhou, F., Chen, Q., Kang, A., Lu, M., Liu, W., Zang, X., Wang, G., Zhang, J., 2015. Chronic inflammation up-regulates P-gp in peripheral mononuclear blood cells via the STAT3/Nf-κb pathway in 2,4,6-trinitrobenzene sulfonic acid-induced colitis mice. Sci. Rep. 5, 13558. https://doi.org/10.1038/srep13558.

Luo, H., Zhang, Y., Guo, H., Zhang, L., Li, X., Ringseis, R., Wen, G., Hui, D., Liang, A., Eder, K., He, D., 2014. Transcriptional regulation of the human, porcine and bovine OCTN2 gene by PPARα via a conserved PPRE located in intron 1. BMC Genet. https://doi.org/10.1186/s12863-014-0090-y.

Luster, M.I., Germolec, D.R., Yoshida, T., Kayama, F., Thompson, M., 1994. Endotoxin-induced cytokine gene expression and excretion in the liver. Hepatology. https://doi.org/10.1002/hep.1840190229.

McKenna, S., Burey, T., Sandoval, J., Nguyen, L., Castro, O., Gudipati, S., Gonzalez, J., El Kasmi, K.C., Wright, C.J., 2018. Immunotolerant p50/NFκB signaling and attenuated hepatic IFNβ expression increases neonatal sensitivity to endotoxemia. Front. Immunol. 9, 2210. https://doi.org/10.3389/fimmu.2018.02210.

Miller, D.S., Bauer, B., Hartz, A.M.S., 2008. Modulation of P-glycoprotein at the blood-brain barrier: opportunities to improve central nervous system pharmacotherapy. Pharmacol. Rev. https://doi.org/10.1124/pr.107.07109.

Morimoto, K., Nakakariya, M., Shirasaka, Y., Kakinuma, C., Fujita, T., Tamai, I., Ogihara, T., 2008. Oseltamivir (Tamiflu) efflux transport at the blood-brain barrier via P-glycoprotein. Drug Metab. Dispos. 36, 6–9. https://doi.org/10.1124/dmd.107.017699.

Nakazawa, Y., Okura, T., Shimomura, K., Terasaki, T., Deguchi, Y., 2010. Drug-drug interaction between oxycodone and adjuvant analgesics in blood-brain barrier transport and antinociceptive effect. J. Pharmacol. Sci. 99, 467–474. https://doi.org/10.1002/jps.21807.

Nežić, L., Škrbić, R., Dobrić, S., Stojiljković, M.P., Šatara, S.S., Milovanović, Z.A., Stojaković, N., 2009. Effect of simvastatin on proinflammatory cytokines production during lipopolysaccharide-induced inflammation in rats. Gen. Physiol. Biophys.

Nicholson, A.N., 1983. Antihistamines and sedation. Lancet (London, England) 2, 211–212.

Nie, W., Sweetser, S., Rinella, M., Green, R.M., 2005. Transcriptional regulation of murine Slc22a1 (Oct1) by peroxisome proliferator agonist receptor-α and -γ. Am. J. Physiol. Gastrointest. Liver Physiol. https://doi.org/10.1152/ajpgi.00057.2004.

Okura, T., Hattori, A., Takano, Y., Sato, T., Hammarlund-Udenaes, M., Terasaki, T., Deguchi, Y., 2008. Involvement of the pyrilamine transporter, a putative organic cation transporter, in blood-brain barrier transport of oxycodone. Drug Metab. Dispos. 36 https://doi.org/10.1124/dmd.108.022087, 2005–2013.

Okura, T., Ito, R., Ishiguro, N., Tamai, I., Deguchi, Y., 2007. Blood–brain barrier transport of pramipexole, a dopamine D2 agonist. Life Sci. 80, 1564–1571. https://doi.org/10.1016/j.lfs.2007.01.035.

Oldendorf, W.H., 1981. Clearance of radiolabeled substances by brain after arterial injection using a diffusible internal standard. Research Methods in Neurochemistry. https://doi.org/10.1007/978-1-4615-7757-7_4.

Oldendorf, W.H., 1970. Measurement of brain uptake of radiolabeled substances using a tritiated water internal standard. Brain Res. 24, 372–376. https://doi.org/10.1016/0006-8993(70)90123-X.

Ose, A., Kusuhara, H., Yamatsugu, K., Kanai, M., Shibasaki, M., Fujita, T., Yamamoto, A., Sugiyama, Y., 2008. P-glycoprotein restricts the penetration of oseltamivir across the blood-brain barrier. Drug Metab. Dispos. 36, 427–434. https://doi.org/10.1124/dmd.107.018556.

Pavese, N., Gerhard, A., Tai, Y.F., Ho, A.K., Turkheimer, F., Barker, R.A., Brooks, D.J., Piccini, P., 2006. Microglial activation correlates with severity in Huntington disease: a clinical and PET study. Neurology 66, 1638–1643. https://doi.org/10.1212/01.wnl.0000222734.56412.17.

Perry, V.H., 2012. Innate inflammation in Parkinson's disease. Cold Spring Harb. Perspect. Med. 2, a009373. https://doi.org/10.1101/cshperspect.a009373.

Poller, B., Drewe, J., Krähenbühl, S., Huwyler, J., Gutmann, H., 2010. Regulation of BCRP (ABCG2) and P-Glycoprotein (ABCB1) by cytokines in a model of the human blood-brain barrier. Cell. Mol. Neurobiol. https://doi.org/10.1007/s10571-009-9431-1.

Qin, L., Wu, X., Block, M.L., Liu, Y., Breese, G.R., Hong, J.-S., Knapp, D.J., Crews, F.T., 2007. Systemic LPS causes chronic neuroinflammation and progressive neurodegeneration. Glia 55, 453–462. https://doi.org/10.1002/glia.20467.

S, L., Chaudhary, S., Ray, R.S., 2017. Hydroalcoholic extract of Stevia rebaudiana bert. leaves and stevioside ameliorates lipopolysaccharide induced acute liver injury in rats. Biomed. Pharmacother. https://doi.org/10.1016/j.biopha.2017.08.082.

S, O., E, N., M, K., Y, S., D, K., 2009. Penetration of oseltamivir and its active metabolite into the brain after lipopolysaccharide-induced inflammation in mice. J. Pharm. Pharmacol. 61 https://doi.org/10.1211/JPP.61.10.0018.

Sadiq, M.W., Borgs, A., Okura, T., Shimomura, K., Kato, S., Deguchi, Y., Jansson, B., Björkman, S., Terasaki, T., Hammarlund-udenaes, M., 2011. Diphenhydramine active uptake at the blood–brain barrier and its interaction with oxycodone in vitro and in vivo. J. Pharmacol. Sci. 100, 3912–3923. https://doi.org/10.1002/jps.22567.

Shaffer, C.L., Osgood, S.M., Mancuso, J.Y., Doran, A.C., 2014. Diphenhydramine has similar interspecies net active influx at the blood-brain barrier. J. Pharmacol. Sci. https://doi.org/10.1002/jps.23927.

Shebl, F.M., Pinto, L.A., García-Piñeres, A., Lempicki, R., Williams, M., Harro, C., Hildesheim, A., 2010. Comparison of mRNA and protein measures of cytokines following vaccination with human papillomavirus-16 L1 virus-like particles. Cancer Epidemiol. Biomark. Prev. 19, 978–981. https://doi.org/10.1158/1055-9965.EPI-10-0064.

Shimomura, K., Okura, T., Kato, S., Couraud, P.-O., Schermann, J.-M., Terasaki, T., Deguchi, Y., 2013. Functional expression of a proton-coupled organic cation (H+/OC) antiporter in human brain capillary endothelial cell line hCMEC/D3, a human blood-brain barrier model. Fluids Barriers CNS 10, 8. https://doi.org/10.1186/2045-8118-10-8.

Somann, J.P., Wasilczuk, K.M., Neihouser, K.V., Sturgis, J., Albors, G.O., Paul Robinson, J., Powley, T.L., Irazoqui, P.P., 2019. Characterization of plasma cytokine response to intraperitoneally administered LPS & subdiaphragmatic branch vagus nerve stimulation in rat model. PloS One 14. https://doi.org/10.1371/journal.pone.0214317.

Spector, R., 1988. Transport of amantadine and rimantadine through the blood-brain barrier. J. Pharmacol. Exp. Therapeut. 244, 516–519.

Sung, B., Park, S., Yu, B.P., Chung, H.Y., 2004. Modulation of PPAR in aging, inflammation, and calorie restriction. Journals Gerontol. Ser. A Biol. Sci. Med. Sci. https://doi.org/10.1093/gerona/59.10.b997.

Suzuki, T., Aoyama, T., Suzuki, N., Kobayashi, M., Fukami, T., Matsumoto, Y., Tomono, K., 2016. Involvement of a proton-coupled organic cation antiporter in the blood-brain barrier transport of amantadine. Biopharm Drug Dispos. 37, 323–335. https://doi.org/10.1002/bdd.2014.

Uno, S., Kawase, A., Tsuji, A., Tanino, T., Iwaki, M., 2007. Decreased intestinal CYP3A and P-glycoprotein activities in rats with adjuvant arthritis. Drug Metabol. Pharmacokinet. 22, 313–321.

Virdis, A., Colucci, R., Fornai, M., Blandizzi, C., Duranti, E., Pinto, S., Bernardini, N., Segnani, C., Antonioli, L., Taddei, S., Salvetti, A., Del Tacca, M., 2005. Cyclooxygenase-2 inhibition improves vascular endothelial dysfunction in a rat model of endotoxic shock: role of inducible nitric-oxide synthase and oxidative stress. J. Pharmacol. Exp. Therapeut. https://doi.org/10.1124/jpet.104.077644.

Vos, T.A., Gouw, A.S.H., Klok, P.A., Havinga, R., Van Goor, H., Huitema, S., Roelofsen, H., Kuipers, F., Jansen, P.L.M., Moshage, H., 1997. Differential effects of nitric oxide synthase inhibitors on endotoxin- induced liver damage in rats. Gastroenterology 113, 1323–1333. https://doi.org/10.1053/gast.1997.v113.pm9322528.

Wang, X., Qi, B., Su, H., Li, J., Sun, X., He, Q., Fu, Y., Zhang, Z., 2017. Pyrilamine-sensitive proton-coupled organic cation (H+/OC) antiporter for brain-specific drug delivery. J. Contr. Release 254, 34–43. https://doi.org/10.1016/j.jconrel.2017.03.034.

Wedn, A.M., El-Gowilly, S.M., El-Mas, M.M., 2020a. Nicotine improves survivability, hypotension, and impaired adenosinergic renal vasodilations in endotoxic rats: role of α7-nAChRs/HO-1 pathway. Shock 53, 503–513. https://doi.org/10.1097/SHK.0000000000001384.

Wedn, A.M., El-Gowilly, S.M., El-Mas, M.M., 2020b. Time and sex dependency of hemodynamic, renal, and survivability effects of endotoxemia in rats. Saudi Pharmaceut. J. 28, 127–135. https://doi.org/10.1016/j.jsps.2019.11.014.

Wen, G., Ringseis, R., Eder, K., 2010. Mouse OCTN2 is directly regulated by peroxisome proliferator-activated receptor α (PPARα) via a PPRE located in the first intron. Biochem. Pharmacol. https://doi.org/10.1016/j.bcp.2009.10.002.

Wright, S.H., Evans, K.K., Zhang, X., Cherrington, N.J., Sitar, D.S., Dantzler, W.H., 2004. Functional map of TEA transport activity in isolated rabbit renal proximal tubules. Am. J. Physiol. Ren. Physiol. 287, F442–F451. https://doi.org/10.1152/ajprenal.00115.2004.

Yao, J., Mackman, N., Edgington, T.S., Fan, S.T., 1997. Lipopolysaccharide induction of the tumor necrosis factor-alpha promoter in human monocytic cells. Regulation by Egr-1, c-Jun, and NF-kappaB transcription factors. J. Biol. Chem. 272, 17795–17801.

Yu, C., Kastin, A.J., Tu, H., Waters, S., Pan, W., 2007. TNF activates P-glycoprotein in cerebral microvascular endothelial cells. Cell. Physiol. Biochem. 20, 853–858. https://doi.org/10.1159/000110445.